Continuum mixture solidification model for simulation of freeze lining in smelting furnace

M. G. Rodrigues, Christian, Montanuniversitaet of Leoben, Austria
Wu, Menghuai, Montanuniversitaet of Leoben, Austria
Ishmurzin, Anton, RHI Magnesita, Austria
Hackl, Gernot, RHI Magnesita, Austria
Voller, Nikolaus, RHI Magnesita, Austria
Ludwig, Andreas, Montanuniversitaet of Leoben, Austria
Kharicha, Abdellah, Montanuniversitaet of Leoben, Austria

Abstract

In pyrometallurgical furnaces, a freeze lining is typically desired to provide a protective layer for the vessels against the corrosive nature of molten slags and extend the operation lifespan of smelters. Most of the understanding of freeze lining behaviour comes from the experience gathered from the metallurgical industries. However, numerical modelling can be an important tool to aid in understanding and predicting the influence of varying operation parameters on the freeze lining formation. In this paper, a continuum mixture solidification model has been used to simulate an industrial electric furnace for nickel smelting, including the formation of the freeze lining. A parameter study has been performed to determine the process window within which a stable freeze lining with a certain thickness is guaranteed during the furnace operation (e.g. with the evolution in feed quantity).

1 Introduction

The concept of freeze lining has been applied to flash furnaces (converting/smelting) (Schlesinger et al., 2011) and electric arc furnaces (smelting/slag cleaning) (Gosselin and Lacroix, 2003; Reynolds and Jones, 2006; Jones and Reynolds, 2002) for many years. The goal was to provide a protective layer for the vessels against the corrosive nature of molten

slags and extend the operation lifespan of smelters (Schlesinger, 1996; Davenport et al., 2002). Cooling elements were typically designed and installed behind the refractory to control the frozen slag layer at the walls. A robust cooling system helps to maximize production, without accelerating the refractory wear (Kyllo et al., 2000).

Most of the existing knowledge about the freeze lining behavior comes from the experience gathered from the metallurgical industries. However, numerical modelling can aid in understanding and predicting the influence of varying operation parameters in the freeze lining formation. Many attempts have been made to simulate the freeze lining formation during the operation of smelting furnaces. Pan et al. (2011) simulated the heat transfer in a six-in-line electric furnaces for smelting sulphide ores to produce base metals and platinum group metals. This simple model only considered the heat transfer, by relating the furnace conditions and performances to various control and input parameters. However, fluid flow simulations were not considered. Sheng et al. (1998a, b, c) coupled the solution of Maxwell's equations (for the electromagnetic stirring force), the Navier-Stokes equations, and the heat transfer equation for the simulation of an electric furnace for nickel smelting. However, slag solidification was not considered. Guevara (2007) used a two-phase numerical model, including Navier-Stokes and energy conservation equations, to analyze different strategies to account for slag solidification. The main focus was to propose numerical correlations to describe the global heat transfer through the wall and the cooling system, as well as through the solid slag layer. However, slag solidification and freeze lining formation were not studied in detail, and to the authors knowledge no further follow-up work of this kind has been reported.

The present article aims to fill the gap in the literature and presents a numerical study of the fluid flow and heat flux of a six-in line electric furnace for nickel smelting. A continuum mixture solidification model was considered, and freeze lining formation was analyzed for a range of furnace conditions.

2 Model description

A one-phase mixture model can be used to describe the solidification of a binary alloy (Voller et al., 1989). This approach is referred to as the continuum mixture model, and has been used to solve the continuity, momentum and energy conservation equations (Table 1, Eqs. 1 to 3). This one-phase model is a simpler and faster version of the Eulerian multiphase models because it solves a smaller number of variables than the corresponding multiphase model. Owing to the large-scale nature of the six-in-line electric smelting furnace (ESF), the continuum mixture solidification model is more appropriate as it provides results with

acceptable accuracy and low computational resources. The mixture density and velocity are written in Eqs. 4 and 5. Solid and liquid volume fractions always add up to 1 ($f_\ell + f_\mathrm{s} = 1$).

Table 1: Conservation equations and list of symbols.

Equations		List of symbols
$\frac{\partial \rho}{\partial t} + \nabla \cdot (\rho \vec{u}) = 0$	(1)	ρ – mixture density $\vec{g}$ – gravity vector
$\frac{\partial}{\partial t}(\rho \vec{u}) + \nabla \cdot (\rho \vec{u}\vec{u}) = \rho \vec{g} - \nabla p + \nabla (\mu \nabla \cdot \vec{u}) + \vec{S}_\mathrm{U}$	(2)	t – time $\vec{u}$ – mixture velocity vector p – static pressure
$\frac{\partial}{\partial t}(\rho h) + \nabla \cdot (\rho \vec{u} h) = \nabla \cdot (k \nabla T) + \rho L \frac{\partial f_\mathrm{s}}{\partial t} + \vec{S}_\mathrm{H}$	(3)	μ – mixture viscosity h – mixture enthalpy k – mixture thermal conductivity
$\rho = f_\ell \rho_\ell + f_\mathrm{s} \rho_\mathrm{s}$	(4)	T – mixture temperature L – latent heat
$\vec{u} = \frac{1}{\rho}(f_\ell \rho_\ell \vec{u}_\ell + f_\mathrm{s} \rho_\mathrm{s} \vec{u}_\mathrm{s})$	(5)	f_s – vol. fraction of solid phase f_ℓ – vol. fraction of liquid phase

The energy conservation equation (Eq. 3) is written according to the enthalpy-porosity approach (Voller and Prakash, 1987) for phase-change problems. The release of latent heat due to slag solidification is captured via the second term on the right-hand-side of Eq. 3. The evolution of f_s is assumed to depend linearly on the temperature:

$$f_\mathrm{s} = (T_\mathrm{liq} - T) / (T_\mathrm{liq} - T_\mathrm{sol}) \qquad (6)$$

where T_liq and T_sol are the liquidus and solidus temperatures. This linear relation between f_s and T is a simplification that will be studied in a future work.

Slag solidification behaves as a porous network (like columnar dendrites in metal alloys), and its solid matrix is assumed to be stationary ($\vec{u}_\mathrm{s} = 0$). Instead of employing a variable viscosity for the slag (which would make the simulation hard to converge), a similar outcome is achieved with the drag term ($\vec{S}_\mathrm{U}$) in Eq. 2:

$$\vec{S}_{\mathrm{U}} = -\frac{\mu_{\ell}}{K}\vec{u} \tag{7}$$

where the permeability K of the mush is given by the Black-Kozeny relation (Gu and Beckermann, 1999):

$$K = \frac{f_{\ell}^{\,3}}{f_{\mathrm{s}}^{\,2}} 6\times 10^{-4} \lambda_1^{\,2} \tag{8}$$

This permeability law is often used in the solidification of alloys with columnar structure, where $\lambda_1^{\,2}$ is the primary dendrite arm spacing. Here, this concept is used for slag solidification. $\vec{S}_{\mathrm{H}}$ in Eq. 3 is the energy source/sink terms, which can be the energy input by the electrode, the energy exhaust due to melting of the feed on the top of the slag bed, or the energy generation due to the matte production at the slag-matte interface. Their modelling is discussed later.

3 Model configuration

A six-electrode ESF was studied. The top and cross-sectional views of the furnace are illustrated in Fig. 1 a) and b). The geometry represents a real industrial case for smelting of Nickel matte. The geometry data have been taken from Sheng et al. (1998 a-c) and Guevara (2007). This work can be considered as an extension of the work of Guevara (2007). The electrode tips are immersed into the molten slag. The electrical energy to smelt the feed is generated by the Joule heating created by the passage of electric current between the carbon electrodes, through the molten slag. According to Sheng et al. (1998a), heat release to the slag is greatest in the near vicinity of the electrodes. After the furnace is charged, slag and matte are produced. The denser matte settles through the liquid slag layer at the bottom of the vessel. The furnace is tapped periodically to discharge the matte and the slag through separate tap holes.

For the simulations, the following assumptions were considered:

1. Because of symmetry, 1/12 of the original furnace is considered.
2. The matte is treated as a pure fluid phase. The slag is also treated as a fluid phase, but the freeze lining can form on the furnace wall, with its solid volume fraction quantified as f_{s}. The domains of slag and matte stay unchanged, i.e. the matte and slag periodical tapping stage is not considered.

3. The flow is laminar.
4. The Boussinesq approximation is used to account for natural convection of the slag (with the reference density and temperature being equal to 2801.7 kg/m^3 and 1416 K, respectively). The magnetohydrodynamic aspects of the flow caused by the presence of the electric current were neglected (Sheng et al., 1998a).
5. A continuous and equal shear stress is assumed at both slag and matte phases sides of the slag-matte interface.
6. The liquid slag is covered by a layer of solid feed.

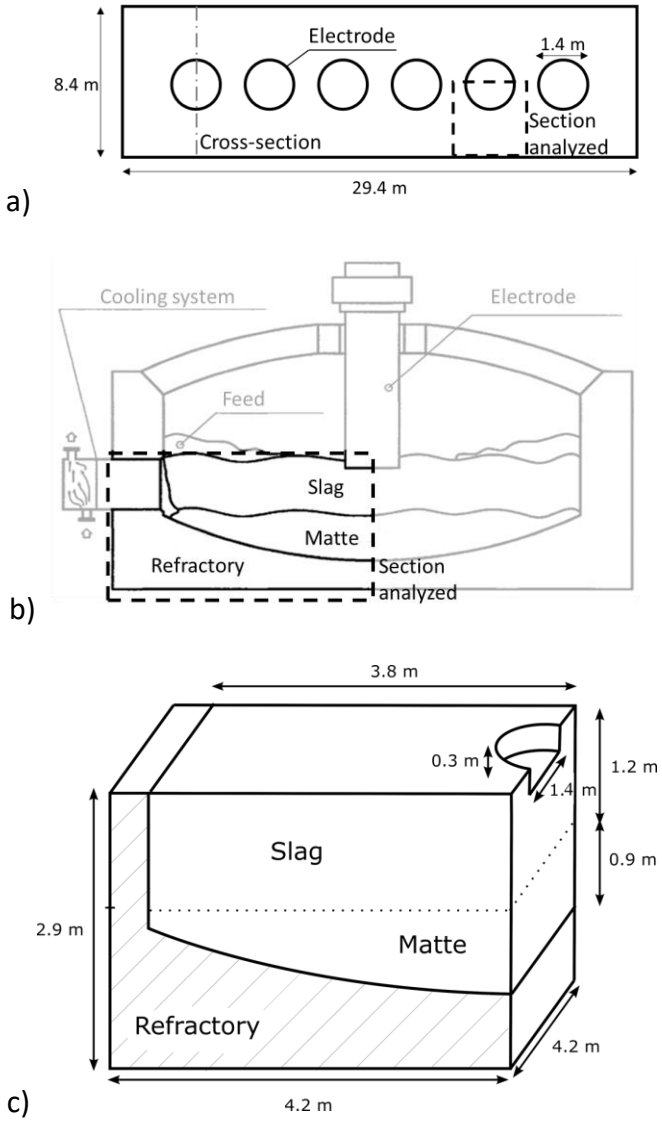

Fig. 1: Schematic of the ESF and configuration of 3D simulation domain: a) top, and b) cross-sectional views of ESF, and c) simulation domain with dimensions

A schematic diagram of the simulation domain and dimensions is shown in Fig. 1 c), whereas the boundary conditions are illustrated in Fig. 2. The refractory is considered by the model, for which only energy equation (Eq. 3) is solved, whereas the matte and the slag are considered as fluid phases, for which both energy and Naiver-Stokes equations are solved (Eqs. 1 to 3). The domain has mesh of around 4 million cells. The material properties are shown in Table 2. Note that an arbitrary primary dendritic arm spacing in the slag phase (Table 2) has been assumed in the permeability expression shown in Eq. 8. This will be subject to review in a later work.

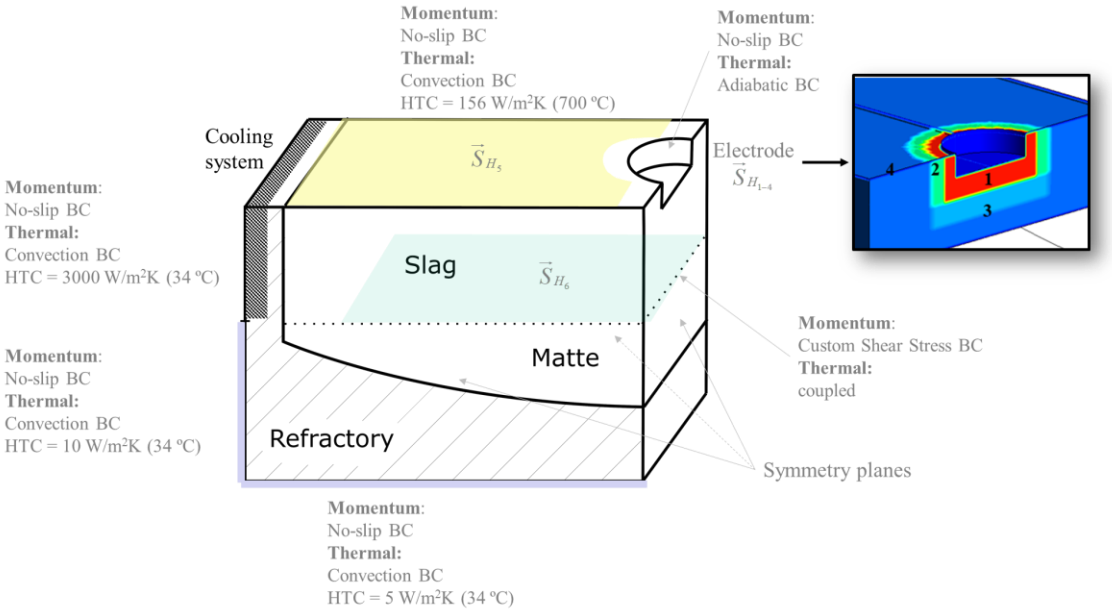

Fig. 2: Boundary conditions for the simulations. Inset illustrates the different zones considered for the energy input from electrode.

Table 2: Material properties used in the simulations.

Slag		
Density, kg/m^3	2801.7 (Boussinesq approximation)	
Thermal Expansion Coefficient, 1/K	9.8×10^{-5}	
Thermal conductivity, W/(m·K)	8.0 ($T<T_{sol}$)	6.5 ($T>T_{liq}$)
Viscosity, kg/(m·s)	0.5	
Specific Heat Capacity, J/(kg·K)	1250	
Liquidus Temperature, K (^{o}C)	1415 (1142)	

Solidus Temperature, K (^{o}C)	1363 (1090)	
Initial Temperature, K	1416	
Latent Heat, J/kg	6.5×10^5	
Primary dendritic arm spacing, m	1.1×10^{-3}	
Matte		
Density, kg/m^3	5100	
Thermal conductivity, W/(m·K)	7.7	
Viscosity, kg/(m·s)	0.004 ($T\geq T_{\mathrm{sol}}$)	3250.0 ($T<T_{\mathrm{sol}}$)
Specific Heat Capacity, J/(kg·K)	600	
Solidus Temperature, K (^{o}C)	1300 (1027)	
Refractory (solid phase)		
Density, kg/m^3	3100	
Thermal conductivity, W/(m·K)	7.7	
Specific Heat Capacity, J/(kg·K)	1260	

For the momentum boundary conditions, a shear stress boundary condition is imposed at the slag-matte interface. This applies the average shear stress between the last layer in the slag region and the first layer in the matte region to guarantee a continuous shear stress profile in the fluid domain. The momentum boundary conditions for the remaining boundaries are no-slip for both of the fluid phases. For the energy equation, convection boundary conditions are assumed at the bottom and side of the refractory, at the cooling system, and at the top of the domain. The specific heat transfer coefficients for each surface in Fig. 2 are based on the work of Guevara (2007). Adiabatic boundary conditions are considered on the electrode surface and symmetry boundary conditions are considered in the remaining surfaces.

The total energy input power in the furnace is *IP*=15 MW. The electrical energy input through the electrodes is dissipated in the slag bath by Joule heating. The dissipation of energy depends on the location in relation to the electrode (Sheng et al., 1998b). Following Guevara (2007), the slag region is divided into 4 zones with weights assigned according to the amount of energy dissipated in each zone. The locations of these zones and their enumeration are illustrated in the inset of Fig. 2. Close to the electrode, a larger weight is considered ($\gamma_1 = 60\%$), and with the distance from the electrode it reduces gradually (i.e.

$\gamma_2 = 25\%$, $\gamma_3 = 10\%$ and $\gamma_4 = 5\%$). The energy source term in each zone is calculated as $\vec{S}_{\mathrm{H}_{1-4}} = \gamma_{1-4} \cdot IP / 12 / V_{1-4}$, where the subscripts 1 to 4 correspond to each of the four zones shown in the inset of Fig. 2. The division by 12 is because the simulation only considers one twelfth of the entire furnace. The integral of the energy release equates the total power input in the section analyzed.

The presence of the feed at the top of the liquid slag region has been associated with an energy sink. It comprises the heat losses by radiation, and the energy dissipated out of the furnace from effluent gases during the furnace operation. The proposed values were derived from a heat balance and depend on the operation conditions of the furnace. For the current furnace IP, an energy sink of $\vec{S}_{\mathrm{H}_5} = 1.67 \times 10^6$ W/m^3 has been used (Guevara, 2007).

The last energy transfer term necessary in the simulation corresponds to a heat source due to the production of matte, which sediments through the slag before settling in the matte. While sedimenting, the hot matte releases heat to the surrounding colder environment. This energy transfer is proportional to the production rate of matte ($\dot{m}$) and the local enthalpy of the system (h). The energy source is given by $\vec{S}_{\mathrm{H}_6} = \dot{m} \cdot h / V_6$. For the current IP, the furnace produces 35 ton of matte per hour (Guevara, 2007) and the average local enthalpy is around 0.7×10^6 J/kg.

4 Results

Three-dimensional temperature distribution is shown in Fig. 3 a) for the entire simulated section. The white line represents the freeze lining solidification front defined as $f_s = 0.1$, i.e. the start of the mushy zone. The mushy zone corresponds to the state between pure liquid and complete solid phase. Notice that, besides the slag and matte regions, the temperature distribution is also shown in the refractory. The most significant heat extraction from the domain occurs in the cooling system and at the top due to the presence of the feed. On the other hand, after reaching a steady-state, the temperature within the bulk slag is fairly uniform, even though the energy input near the electrode is considerable.

The top inset in Fig. 3 a) highlights the temperature distribution in a segment of the furnace that encompasses the refractory (adjacent to the cooling system), the freeze lining and the molten slag. On the bottom inset in Fig. 3 a), the solid fraction contour (varying from 0 in blue to 1 in red) is overlaid with the direction vectors of liquid slag velocity. The completely-

solidified freeze lining is stationary ($\vec{u}_s = 0$). This can be confirmed in this inset, where the velocity vectors disappear as the solid volume fraction increases in the mushy zone.

In Fig. 3 b), the contour of the velocity magnitude is overlaid with the velocity direction vectors in the slag and matte regions. An anti-clockwise flow can be observed in the slag region, which is due to the natural convection from the Joule heating effect created by the electrodes (as shown in the inset of Fig. 2). The motion of the slag causes the matte near the slag-matte interface to flow towards the electrode as a result of the shear stress boundary conditions applied at the slag-matte interface.

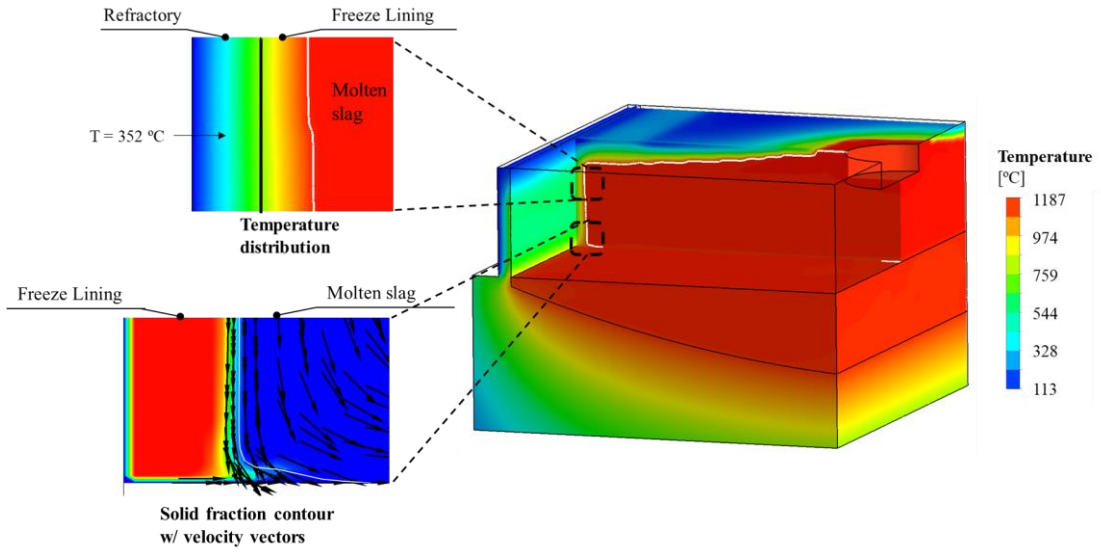

a)

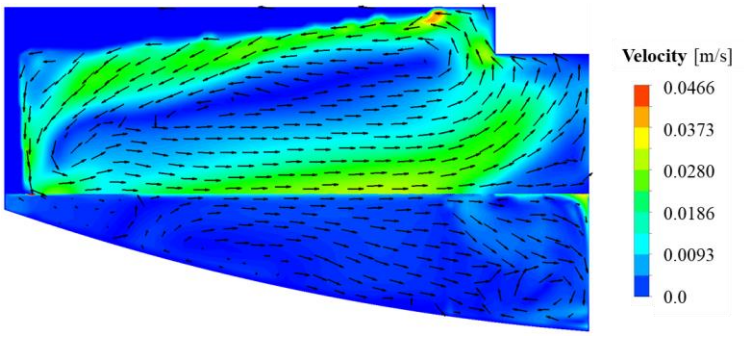

b)

Fig. 3: Contours of a) temperature in 3D domain and b) velocity magnitude in intermediate cross-section of slag and matte regions. White line represents the solidification front ($f_s = 0.1$) in a), whereas vectors represent velocity direction in b). Insets show temperature contour and solid fraction contour overlaid with velocity vectors.

The results of the temperature contour overlaid with the volume rendering of the freeze lining layer in a section of the domain are illustrated in Fig. 4 b). The freeze lining thickness increases towards the slag-matte interface, reaching there a maximum value of around 12 cm.

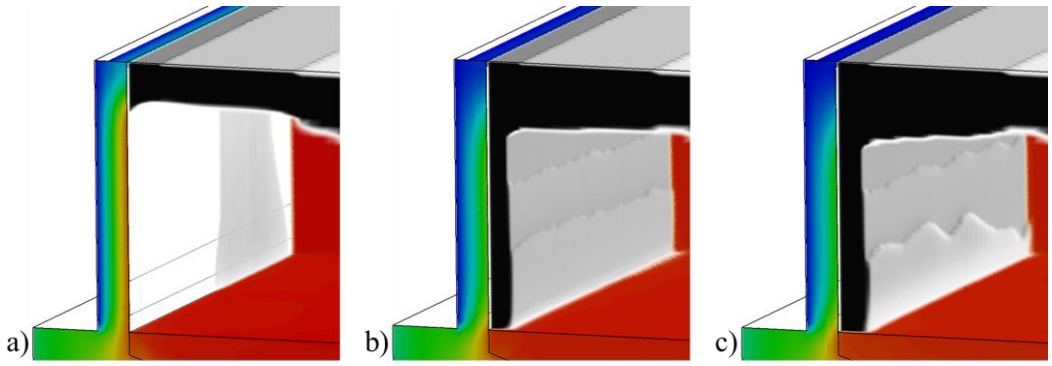

Fig. 4: Freeze lining for different feed quantities: a) $\vec{S}_{H_5} - 10\%$**, b)** $\vec{S}_{H_5}$ **and c)** $\vec{S}_{H_5} + 10\%$**.**

During the smelting process, the feed quantity varies. This is represented by varying $\vec{S}_{H_5}$. The results in Fig. 4 a) and c) show the impact of such variation in the freeze lining formation after decreasing or increasing $\vec{S}_{H_5}$ by 10%, respectively. The reduction of $\vec{S}_{H_5}$ by 10% (Fig. 4 a)) leads to a very dangerous condition (freeze lining is too thin) for the operation of the furnace. On the other hand, increasing $\vec{S}_{H_5}$ by 10% (Fig. 4 c)), the increase in the freeze lining thickness would provide extra protection for the refractory, but would probably not be an ideal solution in terms of the optimal use of the resources in the process.

5 Conclusions

A continuum mixture solidification model has been used to simulate an electric furnace for nickel smelting. The model considers the fluid flow and heat flux in the furnace, as well as the formation of freeze lining. Different freeze lining thicknesses have been predicted for different feed conditions. This reveals that the freeze lining varies with the furnace operation. The results presented here are preliminary of a running project FFG Bridge I - MoSSoFreez. The model will be extended to account for more accurate operation parameters and include a multiphase framework. Also, the linear solidification model (Eq. 6) is going to be extended to include a more realistic, nonlinear dependence of solid fraction on temperature. A better control of the freeze lining during the furnace operation maximizes production, reduces energy consumption and extends the furnace lifespan.

These are important steps in the combat of global warming and reduction of greenhouse gas emissions, following the goals of the last United Nations Climate Change Conference.

Acknowledgement

This study was supported by the Austrian Research Promotion Agency (FFG) in the framework of the MoSSoFreez joint project.

References

M. E. Schlesinger, M. J. King, K. C. Sole, W. G. Davenport, Extractive Metallurgy of Copper, 5th edition, Elsevier Ltd, 2011.

L. Gosselin, M. Lacroix, Heat transfer and banks formation in a slag bath with embedded heat sources, Int. J. Heat Mass Transfer, Vol. 46, 2003, 2537-254.

Q.G. Reynolds, R.T. Jones (Mintek, South Africa), Twin-electrode DC smelting furnaces – Theory and photographic test work, Minerals Engineering, 19 (2006), 325–333

R.T. Jones, Q.G. Reynolds, M.J. Alport (Mintek, South Africa), DC arc photography and modeling, Minerals Engineering, 15 (2002), 985-991.

M.E. Schlesinger: Miner Process Extr Metall Rev, Vol. 16 (2), 1996, 125–40.

W.G. Davenport, M. King, M. Schlesinger, A.K. Biswas, Extractive Metallurgy of Copper (fourth ed.), Elsevier Science Ltd., Oxford, UK, 2002.

A.K. Kyllo, N.B. Gray, D. Papazoglou, B.J. Elliot, Developing Composite Furnace Module Cooling Systems, JOM, Vol. 52 (2), 2000, 66-67.

Y. Pan, S. Sun, S. Jahanshahi, Mathematical modelling of heat transfer in six-in-line electric furnaces for sulphide smelting. J. S. Afr. Inst. Min. Metall. Vol. 111 (10), 2011, 717–732.

Y. Sheng, G. Irons, and D. Tisdale, Transport phenomena in electric smelting of nickel matte: Part I. Electric potential distribution, Metall. Mater. Trans. B, Vol. 29, 1998a, 77–83.

Y. Sheng, G.A. Irons, D. Tisdale, Transport phenomena in electric smelting of nickel matte: Part II. Mathematical modeling, Metall. Mater. Trans. B, Vol. 29, 1998b, 85–94.

Y. Sheng, G. Irons, Mathematical and physical modelling of fluid flow and heat transfer in electric smelting, Can. Metall. Q., Vol. 37, 1998c, 265-273.

F. Guevara, Study of slag freezing in metallurgical furnaces, PhD thesis, McMaster Univ., Mar. 2007.

V. R. Voller, A. D. Brent, C. Prakash, The modelling of heat, mass and solute transport in solidification systems, Int. J. Heat Mass Transfer, Vol. 32, No 9, 1989, 1719-1731.

V. R. Voller, C. Prakash, Fixed grid numerical modelling methodology for convection-diffusion mushy region phase-change problems, Int. J. Heat Mass Transfer, Vol. 30, No 8, 1987, 1709-1719.

J. P. Gu, C. Beckermann, Simulation of convection and macrosegregation in a large steel ingot, Metall. Mater. Trans. A, Vol. 30A, 1999, 1357-1366.